CMS Physics Analysis Summary

Contact: cms-pag-conveners-smp@cern.ch 2016/08/04

Measurement of the production cross section for $pp \to Z\gamma \to \nu\bar{\nu}\gamma$ at $\sqrt{s} = 13$ TeV at CMS

The CMS Collaboration

Abstract

A measurement of the $Z\gamma \to \nu\bar{\nu}\gamma$ cross section in pp collisions at $\sqrt{s} = 13\,\text{TeV}$ is presented, using data corresponding to an integrated luminosity of $2.3\,\text{fb}^{-1}$ collected with the CMS detector at the LHC. Events are selected requiring a single photon with transverse momentum above 175 GeV within the pseudorapidity range $|\eta| < 1.44$ accompanied by missing transverse energy above 170 GeV. The measured $Z\gamma \to \nu\bar{\nu}\gamma$ production cross section, 66.5 ± 13.6 (stat) $\pm$ 14.3 (syst) $\pm$ 2.2 (lumi) fb for a single photon with transverse momentum above 175 GeV within the pseudorapidity range $|\eta| < 1.44$, agrees within uncertainties with the next-to-next-to-leading order standard model prediction of 65.5 ± 3.3 fb.

1 Introduction

The study of the production of boson pairs provides an important test of the electroweak sector of the standard model (SM). This production is sensitive to trilinear gauge boson self-interaction couplings (TGCs), a consequence of the non-Abelian nature of the $SU(2) \times U(1)$ symmetry. The values of these couplings are fixed in the SM, and thus, any measured deviation from the SM prediction would be an indication of new physics at the vertex involving the bosons [1, 2]. New symmetries or new particles would give rise to non-zero values of these couplings with cross sections different from the SM prediction, particularly for high energy bosons.

In this paper, we describe the measurement of the cross section for a Z boson produced in association with a photon, with the Z boson decaying to a pair of neutrinos. We used an integrated luminosity of 2.3 fb^{-1} at a center of mass energy of $\sqrt{s} = 13\,\text{TeV}$, extending previous measurements performed at $\sqrt{s} = 7\,\text{TeV}$ and 8 TeV [3, 4].

The $\nu\bar{\nu}\gamma$ final state can be produced through initial-state radiation, where a photon is emitted by an initial-state parton, or through anomalous coupling vertices. The allowed tree-level diagram in the SM for $Z\gamma$ production in pp collisions is shown in Fig. 1.

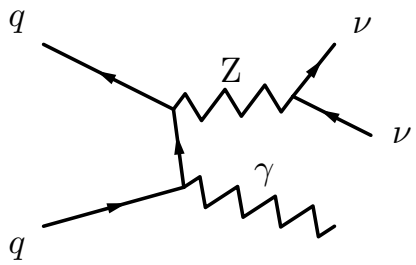

Figure 1: The tree-level Feynman diagram for $Z\gamma$ production via initial state radiation in the SM.

The fiducial phase space for this measurement is defined by the requirements of photon transverse energy $E_{\text{T}}^{\gamma} > 175\,\text{GeV}$ and photon pseudorapidity $|\eta^{\gamma}| < 1.44$. The pseudorapidity requirement reduces the contamination from other particles misidentified as photons [5].

2 The CMS detector and particle reconstruction

The central feature of the CMS apparatus is a superconducting solenoid of 6 m internal diameter, providing a magnetic field of 3.8 T. Within the superconducting solenoid volume are a silicon pixel and strip tracker, a lead tungstate crystal electromagnetic calorimeter (ECAL), and a brass and scintillator hadron calorimeter (HCAL), each composed of a barrel ($|\eta| < 1.479$) and two endcap ($1.479 < |\eta| < 3.0$) sections. Extensive forward calorimetry complements the coverage provided by the barrel and endcap detectors. Muons are measured in gas-ionization detectors embedded in the steel flux-return yoke outside the solenoid. The energy resolution for photons with transverse momentum above 60 GeV varies between 1% and 2.5% over the solid angle of the ECAL barrel, and from 2.5% to 3.5% in the endcaps [5]. The timing measurement of the ECAL has a resolution better than 200 ps for energy deposits larger than 10 GeV [5].

In the η-ϕ plane and for $|\eta| < 1.48$, the HCAL cells map onto 5×5 arrays of ECAL crystals to form calorimeter towers projecting radially outward from the nominal interaction point.

The event reconstruction is performed using a particle-flow (PF) algorithm [6, 7], which reconstructs and identifies individual particles using an optimized combination of information from all subdetectors. Photons are identified as energy clusters in the ECAL by a cluster reconstruction algorithm that consists of three steps. First, cluster seeds are identified as local energy maxima above a given threshold. Second, topological clusters are grown from the seeds by aggregating crystals with at least one side in common with a clustered crystal, and with an energy in excess of a given threshold. These thresholds represent about two standard deviations of the electronic noise in the ECAL (i.e. 80 MeV in the barrel and up to 300 MeV in the endcaps, depending on $|\eta|$). Finally, the clusters are dynamically merged into "superclusters". The merging allows for good energy containment, provides robustness against a high number of additional proton-proton interactions (pileup) in the same bunch crossing, and accounts for geometrical variations with η in the detector. The energy of charged hadrons is determined from a combination of the track momentum and the corresponding ECAL and HCAL energies, corrected for the combined response function of the calorimeters. The energy of neutral hadrons is obtained from the corresponding corrected ECAL and HCAL energies. For each event, hadronic jets are formed from these reconstructed particles with the infrared- and collinear-safe anti-k_t algorithm [8], using a distance parameter $\Delta R = 0.4$, where $\Delta R = \sqrt{(\Delta\eta)^2 + (\Delta\phi)^2}$. The missing transverse momentum vector $\vec{E}_{\mathrm{T}}^{\mathrm{miss}}$ is defined as the projection on the plane perpendicular to the beams of the negative vector sum of the momenta of all reconstructed PF candidates in an event; its magnitude is referred to as $E_{\mathrm{T}}^{\mathrm{miss}}$.

A more detailed description of the CMS detector, together with a definition of the coordinate system used and the relevant kinematic variables, can be found in Ref. [9].

3 Event selection

Events are selected using a single-photon trigger that requires a photon with transverse energy $E_{\mathrm{T}}^{\gamma} > 165\,\mathrm{GeV}$. The trigger is 98% efficient for events in the fiducial phase space of this analysis, $E_{\mathrm{T}}^{\gamma} > 175\,\mathrm{GeV}$ and $|\eta^{\gamma}| < 1.44$ [10]. Photon candidates are restricted to be in the barrel region, where the signal to background ratio is highest.

To distinguish photons from misidentified jets, we apply additional requirements on the energy deposits in the calorimeter. The hadronic energy associated with the photon supercluster should not exceed 5% of its energy as measured in the ECAL. In addition, the photon candidates must have a lateral shower distribution in the ECAL consistent with that expected for an electromagnetic (EM) particle [10]. To further reduce photon contamination arising from misidentified jets, isolation requirements on photon candidates are imposed. Isolation deposits are obtained by considering particles in a cone around the axis defined by the supercluster position and the primary vertex [10]. In particular, the scalar sum of the transverse momenta of all PF photons that are not in the area of the supercluster of the candidate photon, but are within a cone of $\Delta R = 0.3$ around the photon, is required to be less than $(0.28 + 0.0053 \times p_{\mathrm{T}}^{\gamma})$ GeV. In addition, the scalar sum of the transverse momenta of all PF charged hadrons within a cone of $\Delta R = 0.3$ that are associated with the primary vertex and not associated with the candidate photon, is required to be less than 1.37 GeV. Finally, the scalar sum of the transverse momentum magnitude of all PF neutral hadrons within a cone of $\Delta R = 0.3$ of the candidate photon is required to be less than $(1.06 + 0.014 \times p_{\mathrm{T}}^{\gamma} + 0.000019 \times p_{\mathrm{T}}^{\gamma 2})\,\mathrm{GeV}$. Due to the high pileup conditions at the LHC, it is difficult to know the true interaction vertex of the photon for a

$\gamma + E_{\mathrm{T}}^{\mathrm{miss}}$ final state, which could lead to an underestimation of isolation values. Therefore, an additional PF isolation is computed with the charged hadrons from each vertex, and the largest value of this isolation sum is required to be smaller than the nominal threshold used for charged particle isolation.

In each event the highest-energy crystal within the EM shower of the photon candidate is required to be within ± 3 ns of the time expected for particles from a collision. This requirement reduces the background rate arising from showers produced by bremsstrahlung from muons associated with the beam and travelling parallel to the beam line (beam halo), or coming from cosmic rays. To further reduce this background, we exploit the characteristic signature of showers from beam halo in the ECAL. A search region is defined around the highest energy (seed) crystal of the EM cluster in a narrow ϕ window and over a wide η range, after removal of the EM shower in a 5×5 array around the seed crystal. A fit is performed over the remaining cells within this region by a straight line, parallel to the beam direction. Events are tagged as containing a minimum ionizing particle (MIP tag) if the total energy deposited in the crystals associated with the straight-line fit is greater than 4.9 GeV.

Photon candidates are also removed if they are likely to be electrons, as inferred from characteristic patterns of hits in the pixel detector that are associated to the EM clusters [11]. This is called the "pixel seed" criteria. After the above mentioned selection criteria, events are required to have $E_{\mathrm{T}}^{\mathrm{miss}} > 170$ GeV. A topological requirement of $\Delta\phi > 2$ radians between the direction of the photon candidate and the vector $\vec{E}_{\mathrm{T}}^{\mathrm{miss}}$ is applied to reduce the contribution from the γ+jet background. Events are rejected if they contain significant leptonic activity, defined as a lepton (an electron or a muon) with $p_{\mathrm{T}} > 10$ GeV that is $\Delta\mathrm{R} > 0.5$ away from the photon. A requirement of $\Delta\phi < 0.5$ between the jet and $E_{\mathrm{T}}^{\mathrm{miss}}$ is applied to reject events with $E_{\mathrm{T}}^{\mathrm{miss}}$ induced by mismeasurement of the jet energy in the γ+jet background, where the jet is selected by requiring $p_{\mathrm{T}} > 30$ GeV and $|\eta| < 5.0$.

After applying all of the selection criteria, 77 candidate events are found in data.

4 Signal and background modeling

The final state consisting of an energetic photon accompanied by an imbalance in transverse energy can be mimicked by several other SM processes. These processes include $\mathrm{W}\gamma \to \ell\nu\gamma$ where ℓ is a charged lepton (if the lepton escapes detection), $\mathrm{W} \to \ell\nu$ (if the lepton is misidentified as a photon), $\gamma +$ jets (if the jets are misreconstructed, resulting in $E_{\mathrm{T}}^{\mathrm{miss}}$), QCD multijet production including $\mathrm{Z} \to \nu\bar{\nu} +$ jets (if a jet is misidentified as a photon), $\mathrm{Z}\gamma \to \ell^+\ell^-\gamma$ (if both leptons escape detection), and also backgrounds from beam halo or spurious ECAL signals, the latter of which are due to highly ionizing particles interacting with the electronics.

The analysis strategy consists of using observed data to measure those major SM backgrounds that are not modeled accurately in the simulation. Such backgrounds generally are not well constrained by experiment and include fragmentation and misidentification of a jet or an electron as a photon. The dominant background contribution estimated using simulated events arises from $\mathrm{W}\gamma \to \ell\nu\gamma$ production. Smaller contributions from $\gamma +$ jets, $\mathrm{Z}\gamma \to \ell^+\ell^-\gamma$, $\mathrm{W} \to \mu\nu$, $\mathrm{W} \to \tau\nu$ and $\mathrm{t\bar{t}}\gamma$ processes are also estimated using simulation. Samples for these backgrounds are generated with PYTHIA 8.2 [12] and MADGRAPH5_aMC@NLO v2.2 [13].

The cross section for the SM $\mathrm{W}\gamma \to \ell\nu\gamma$ background is corrected with the cross section computed at next-to-next-to-leading order (NNLO) in pQCD. The cross section for $\mathrm{W}\gamma \to \ell\nu\gamma$ with photon transverse momentum above 175 GeV at NNLO is predicted to be 243 ± 17 fb [14,

15]. To estimate the efficiency for the SM $Z\gamma$ measurement, events are generated with the MADGRAPH5_aMC@NLO generator at leading order (LO) with up to two jets, employing NNPDF3.0 LO ($\alpha_S = 0.130$) as the parton distribution function [16]. The p_T distribution in simulation is corrected with the differential cross section for $Z\gamma$ at NNLO [14, 15]. Additionally, to account for rate suppression due to higher-order electroweak effects at high vector boson p_T, correction factors taken from Refs. [17] and [18] are applied to both the $W\gamma \to \ell\nu\gamma$ and $Z\gamma$ samples as a function of the photon p_T. The electroweak corrections are of the order of 5–30%, 5–20% for $Z\gamma$ and $W\gamma \to \ell\nu\gamma$, respectively, in the p_T range considered. The $\gamma +$ jets sample is normalized using the next-to-leading order (NLO) cross section.

In all cases, the underlying event and pile-up particles contribution is included, the energy depositions in various parts of the detector are simulated using GEANT4 [19, 20] and the detector response is simulated using CMS code to produce raw data, which is ultimately reconstructed in the same software as is used for collision data.

To account for differences arising from imperfect modeling of the data in the simulation, a total correction factor $\rho = 0.99 \pm 0.08$ is applied to all backgrounds estimated from simulation, where ρ is the product of individual correction factors defined as ratios of the efficiencies measured in data and in simulation. These ratios include a correction of 0.99 ± 0.02 for the modeling of photon identification, measured using $Z \to e\bar{e}$ events, and 1.00 ± 0.02 for the modeling of pixel seed, measured using $Z \to e\bar{e}$ events. Another ratio is assessed for the combination of several requirements: the PF isolation computed from the charged hadron having the largest isolation sum, the MIP tag, and the rejection of events with additional leptons. This ratio is measured to be 1.00 ± 0.08 using $Z\gamma \to \mu^+\mu^-\gamma$ events.

5 Background estimation

The $W\gamma \to \ell\nu\gamma$ background estimate after the full event selection is found be 10.60 ± 1.58 events, where the uncertainty includes statistical and systematic components. For the systematic uncertainty in the $W\gamma \to \ell\nu\gamma$ estimates, four sources are considered. Firstly, the parton density function (PDF) and QCD scale uncertainties are determined to be 5.4% and 8.9%, respectively. Secondly, the electroweak correction uncertainties are estimated to be the size of the full correction, which is 7.0%. Thirdly, the uncertainty in the correction factor ρ, is determined to be 8.0% as described in Section 4. Finally, the systematic uncertainty due to potential mismodeling of the jet, E_T^{miss}, and photon energy scales, as well as pileup, is found to be 6.2%.

The other backgrounds estimated from simulation include $\gamma +$ jets, $Z\gamma \to \ell^+\ell^-\gamma$, $W \to \mu\nu$, $W \to \tau\nu$ and $t\bar{t}\gamma$. These backgrounds constitute a small fraction of the total background expectation. The total number of events is estimated to be 3.03 ± 0.69 after the full selection, where the uncertainty includes the statistical and systematic uncertainties due to the correction factor ρ and mismodeling of reconstructed objects.

The background originating from jets misidentified as photons is estimated from data. The method is based on a class of jets, referred to as "photon-like" jets, that have properties similar to electromagnetic objects. Photon-like jets are required to pass a very loose photon selection but at the same time fail one of the isolation requirements. The method is based on the measurement of the ratio of jets passing the full photon selection to those identified as photon-like jets. This ratio is applied as a weight to the events passing the loose selection in order to estimate the misidentified contribution passing the full selection. This ratio is measured in a control sample enriched in QCD multijet events. To suppress the contribution of electroweak processes, the missing transverse energy in this control sample is required to be smaller than 30 GeV. This

sample also contains prompt isolated photons from QCD direct photon production; this contribution is subtracted from the numerator of the ratio. The required correction is estimated by performing a fit to the distribution of the width of the shower in pseudorapidity [5]. Two shower shape profiles are used in this fit. The first is the shower shape of prompt photons, obtained from simulated γ + jets events. The second is the shower shape of photon-like jets obtained from a 7–13 GeV sideband of the charged hadron isolation distribution. The number of background events from jets misidentified as photons is measured to be 1.7 ± 0.6, where the uncertainty includes uncertainty in the ratio due to sample purity, different $E_{\mathrm{T}}^{\mathrm{miss}}$ selections for defining the control region of $E_{\mathrm{T}}^{\mathrm{miss}} < 30$ GeV, alternate definitions of the photon-like jet object criteria and the statistical uncertainty (dominant) in the sample used to make the final estimate. The shape of the signal template is also checked in $\mathrm{Z}\gamma \to \mu^+\mu^-\gamma$ events in data and the difference from the signal template in the simulation is found to be negligible relative to the background uncertainty.

An instrumental background from electrons arises due to the inefficiency of reconstructing a hit in the pixel associated with the electron, resulting in the misidentification of the electron as a photon. For our kinematic requirements, this background largely originates from W boson ($\mathrm{W} \to \mathrm{e}\nu$) production and is estimated from the data. The pixel seed efficiency, $\varepsilon_{\mathrm{pix}}$, is measured using the tag-and-probe method [21] and is estimated to be 0.972 ± 0.002 for electrons with $p_{\mathrm{T}} > 100$ GeV. To estimate the final yield of this background, a factor of $(1\text{-}\varepsilon_{\mathrm{pix}})/\varepsilon_{\mathrm{pix}}$ is applied to a set of events in the data with the same selection as the signal candidates, except that they are required to have associated hits in the pixel detector. The resulting contribution is estimated to be 7.8 ± 1.8 events, where the uncertainty is dominated by the uncertainty from the measurement of $\varepsilon_{\mathrm{pix}}$.

Because photon candidates are only identified within the ECAL, selected events are susceptible to contamination from non-collision backgrounds. These backgrounds arise from material interactions with accelerator-related particles (beam halo), spurious signals in the ECAL itself, and particles originating from cosmic ray interactions. The timing distribution measured from the ECAL for each of these backgrounds is different from the arrival time distribution from photons produced in collisions. A fit is performed to the candidate time distribution, using profiles taken from data. The profile distributions of beam halo events are constructed by tagging the events using the MIP tag and spurious ECAL signals by requiring a low value of the shower shape variable. The arrival time for photons from the interaction region is modeled using data $\mathrm{W} \to \mathrm{e}\nu$ candidates. Residual backgrounds from beam halo and spurious signals in the ECAL are significant and contribute 5.9 ± 4.7 and 5.6 ± 2.2 events, respectively, to the signal region. The uncertainty on these values is dominated by the statistical component.

6 Systematic uncertainties

The largest experimental systematic uncertainty on the $Z\gamma$ cross section measurement (which has a small yield relative to the number of expected signal events) is the uncertainty in events with objects misidentified as photons. These events include jets fragmenting to photons, electrons with missing tracks, energy deposits from beam halo particles, and spurious ECAL signals.

The theoretical uncertainties that contribute to the extraction of the measured cross section arise from imprecise knowledge of parton density function , from the choice of QCD scales and electroweak corrections. The magnitude of the PDF uncertainty is estimated according to the LHAPDF prescription [22] using the NNPDF3.0 LO as PDF. The QCD scale uncertainty is determined by raising and lowering the magnitude of the renormalization and factorization

scales by a factor of two. The electroweak correction factors are taken from Refs. [17] and [18] and their uncertainty is the largest theoretical uncertainty on the measured cross section.

An additional source of uncertainty in the measured cross section is smearing and scaling of distributions from uncertainty in the photon and $E_{\mathrm{T}}^{\mathrm{miss}}$ energy scales. The calibration of the reconstructed Z boson mass is used to derive scale factors for the electron energy scale. The differences between the electron and photon energy scales are corrected using simulation. The uncertainty on the photon energy scale is estimated to be 1.5%. The uncertainty on the $E_{\mathrm{T}}^{\mathrm{miss}}$ is due to the uncertainties in the measured PF candidate four-momentum. The charged hadron momentum uncertainty is dominated by the tracker resolution. The photon energy scale is calibrated using the π^0 mass and the Z mass with electron-to-photon correction factors. The neutral hadron energy has the largest uncertainty. Individual PF candidate momenta and energy are varied within $\pm 1\sigma$ of their uncertainties to determine the $E_{\mathrm{T}}^{\mathrm{miss}}$ uncertainty. Subdominant uncertainties in the trigger and reconstruction efficiency of photons are determined using the tag-and-probe technique with $\mathrm{Z} \to \mathrm{e}^{+}\mathrm{e}^{-}$ events. The photon and $E_{\mathrm{T}}^{\mathrm{miss}}$ reconstruction uncertainties together translate into an uncertainty of 6% in $\mathcal{A} \times \varepsilon$, where $\mathcal{A}$ is the acceptance and ε is the efficiency. The uncertainty on the integrated luminosity is 2.7% [23]. A summary of the systematic uncertainties on the cross section is shown in Table 1.

Sources	Effect on cross section (%)
Luminosity	3.3
PDF and QCD scale	6.8
Electroweak corrections	11.3
Jets misidentified as γ	1.3
Electron misidentified as γ	3.6
Beam halo	11.0
Spurious ECAL signals	5.0
$E_{\mathrm{T}}^{\mathrm{miss}}$, photon energy scales, pileup	7.1
Data/sim. scale factors	9.7

Table 1: Summary of systematic uncertainties on the cross section in %. Data/simulation scale factors include a correction for the modeling of photon identification, pixel seed and for the combination of several requirements: the PF isolation computed from the charged hadron having the largest isolation sum, the MIP tag, and the rejection of events with additional leptons.

7 Cross section measurement

The cross section at next-to-next-to-leading order is predicted to be 65.55 ± 3.3 fb [14, 15], where the uncertainty includes only QCD scale variations. The expected number of $\mathrm{Z}\gamma \to \nu\bar{\nu}\gamma$ signal events, 41.7 ± 6.7, is obtained using MADGRAPH5_aMC@NLO at LO with up to two additional jets, where the differential p_{T} distribution is normalized to the NNLO predicted cross section. The total number of expected background events is 34.7 ± 5.8. A summary of the backgrounds and data yields is given in Table 2, where the uncertainties in the background estimates include both statistical and systematic sources.

The distributions of photon transverse energy and $E_{\mathrm{T}}^{\mathrm{miss}}$ are given in Fig. 2, with the signal and background predictions overlaid. No excess of events is observed above the standard model expectation, within uncertainties.

The $\mathrm{Z}\gamma \to \nu\bar{\nu}\gamma$ cross section for $E_{\mathrm{T}}^{\gamma} > 175\,\mathrm{GeV}$ and $|\eta| < 1.44$ is calculated using the following formula:

$$\sigma \times \mathcal{B} = \frac{N_{\mathrm{data}} - N_{\mathrm{bg}}}{\mathcal{A} \times \epsilon \times \mathcal{L}},$$

where N_{data} is the number of observed events, N_{bg} is the estimated number of background events, $\mathcal{A}$ is the geometrical and kinematic acceptance of the selection criteria, ϵ is the sig-

Process	Estimate
$Z\gamma \to \nu\bar{\nu}\gamma$	41.74 ± 6.67
$W\gamma \to \ell\nu\gamma$	10.60 ± 1.58
$W \to e\nu$	7.80 ± 1.78
Jet $\to \gamma$ misidentified	1.75 ± 0.61
Beam halo	5.90 ± 4.70
Spurious ECAL signals	5.63 ± 2.20
Rare backgrounds	3.03 ± 0.69
Total Expectation	76.45 ± 8.82
Data	77

Table 2: Summary of estimated backgrounds and observed total number of candidates for 2.3 fb^{-1} at 13 TeV. Other rare backgrounds include the contributions from the γ + jets, $Z\gamma \to \ell^+\ell^-\gamma$, $W \to \mu\nu$, $W \to \tau\nu$ and $t\bar{t}\gamma$ processes.

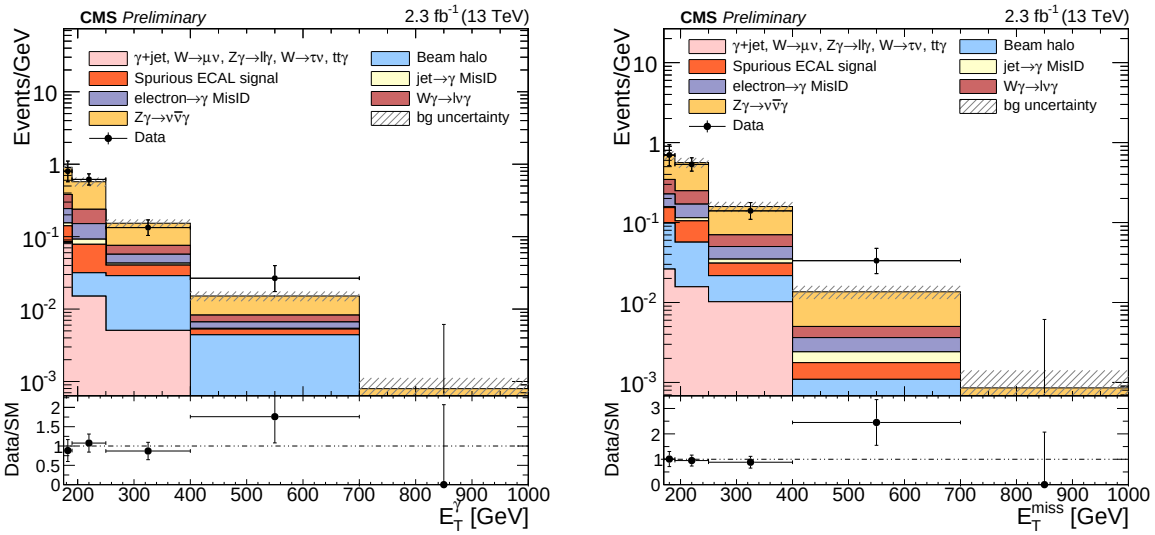

Figure 2: The E_T^γ (left) and E_T^{miss} (right) distributions in data (points with error bars) compared with the SM $Z\gamma \to \nu\bar{\nu}\gamma$ signal and estimated contributions from backgrounds. The background uncertainty includes statistical and systematic components.

nal selection efficiency, and $\mathcal{L}$ is the integrated luminosity. The calculation of $\mathcal{A}$ accounts for the residual photon resolution effects at the kinematic edges of the allowed phase space. The product of $\mathcal{A} \times \epsilon$ is estimated from the simulation to be 0.279 $\pm$ 0.002 (stat) $\pm$ 0.042 (syst), where the systematic uncertainties include those listed in Table 1 for $Z\gamma \to \nu\bar{\nu}\gamma$. In the regime of $p_T^\gamma > 175$ GeV and $|\eta^\gamma| < 1.44$, the measured production cross section for $Z\gamma \to \nu\bar{\nu}\gamma$ is $66.5 \pm 13.6\,(\text{stat}) \pm 14.3\,(\text{syst}) \pm 2.2\,(\text{lumi})$ fb, which is in agreement with the theoretical cross section, predicted at NNLO, of 65.5 ± 3.3 fb [14, 15].

8 Summary

A measurement of the $Z\gamma \to \nu\bar{\nu}\gamma$ cross section in pp collisions at $\sqrt{s} = 13$ TeV is presented, using data corresponding to an integrated luminosity of 2.3 fb^{-1} collected with the CMS detector at the LHC. Events are selected requiring a single photon with transverse momentum above 175 GeV within the pseudorapidity range $|\eta| < 1.44$ accompanied by missing transverse en-

ergy above 170 GeV. The measured $Z\gamma \to \nu\bar{\nu}\gamma$ production cross section, $66.5 \pm 13.6\,(\text{stat}) \pm 14.3\,(\text{syst}) \pm 2.2\,(\text{lumi})$ fb, agrees within uncertainties with the next-to-next-to-leading order standard model prediction of 65.5 ± 3.3 fb.

References

[1] J. Ellison and J. Wudka, "Study of trilinear gauge-boson couplings at the Tevatron collider", *Ann. Rev. Nucl. Part. Sci.* **48** (1998) 33, doi:10.1146/annurev.nucl.48.1.33.

[2] K. Hagiwara, R. D. Peccei, and D. Zeppenfeld, "Probing the weak boson sector in $e^+e^- \to W^+W^-$", *Nucl. Phys. B* **282** (1987) 253, doi:10.1016/0550-3213(87)90685-7.

[3] CMS Collaboration, "Measurement of the production cross section for $Z\gamma \to \nu\bar{\nu}\gamma$ in pp collisions at $\sqrt{s} = 7$ TeV and limits on $ZZ\gamma$ and $Z\gamma\gamma$ triple gauge boson couplings", *JHEP* **1310** (2013) 164, doi:10.1007/JHEP10(2013)164, arXiv:1309.1117.

[4] CMS Collaboration, "Measurement of the production cross section for $Z\gamma \to \nu\bar{\nu}\gamma$ in pp collisions at $\sqrt{s} = 8$ TeV and limits on $ZZ\gamma$ and $Z\gamma\gamma$ triple gauge boson couplings", CMS Physics Analysis Summary SMP-14-019, 2015.

[5] CMS Collaboration, "Performance of Photon Reconstruction and Identification with the CMS Detector in Proton-Proton Collisions at $\sqrt{s} = 8$ TeV", *JINST* **10** (2015) P08010, doi:10.1088/1748-0221/10/08/P08010, arXiv:1502.02702.

[6] CMS Collaboration, "Particle-Flow Event Reconstruction in CMS and Performance for Jets, Taus, and MET", CMS Physics Analysis Summary PFT-09-001, 2009.

[7] CMS Collaboration, "Commissioning of the Particle-Flow reconstruction in Minimum-Bias and Jet Events from pp Collisions at 7 TeV", CMS Physics Analysis Summary PFT-10-002, Geneva, 2010.

[8] M. Cacciari, G. P. Salam, and G. Soyez, "The anti-k_t jet clustering algorithm", *JHEP* **04** (2008) 063, doi:10.1088/1126-6708/2008/04/063, arXiv:0802.1189.

[9] CMS Collaboration, "The CMS experiment at the CERN LHC", *JINST* **3** (2008) S08004, doi:10.1088/1748-0221/3/08/S08004.

[10] CMS Collaboration, "Performance of photon reconstruction and identification with the CMS detector in proton-proton collisions at $\sqrt{s} = 8$ TeV", *JINST* **10** (2015), no. 08, P08010, doi:10.1088/1748-0221/10/08/P08010, arXiv:1502.02702.

[11] CMS Collaboration, "Performance of electron reconstruction and selection with the CMS detector in proton-proton collisions at $\sqrt{s} = 8$ TeV", *JINST* **10** (2015), no. 06, P06005, doi:10.1088/1748-0221/10/06/P06005, arXiv:1502.02701.

[12] T. Sjstrand et al., "An Introduction to PYTHIA 8.2", *Comput. Phys. Commun.* **191** (2015) 159–177, doi:10.1016/j.cpc.2015.01.024, arXiv:1410.3012.

[13] J. Alwall et al., "The automated computation of tree-level and next-to-leading order differential cross sections, and their matching to parton shower simulations", *JHEP* **07** (2014) 079, doi:10.1007/JHEP07(2014)079, arXiv:1405.0301.

[14] M. Grazzini, S. Kallweit, D. Rathlev, and A. Torre, "$Z\gamma$ production at hadron colliders in NNLO QCD", *Phys. Lett. B* **731** (2014) 204–207, doi:10.1016/j.physletb.2014.02.037, arXiv:1309.7000.

[15] M. Grazzini, S. Kallweit, and D. Rathlev, "Wgamma and Zgamma production at the LHC in NNLO QCD", in *Proceedings, 12th International Symposium on Radiative Corrections (Radcor 2015) and LoopFest XIV (Radiative Corrections for the LHC and Future Colliders)*. 2016. arXiv:1601.06751.

[16] NNPDF Collaboration, "Parton distributions for the LHC Run II", *JHEP* **04** (2015) 040, doi:10.1007/JHEP04(2015)040, arXiv:1410.8849.

[17] A. Denner, S. Dittmaier, M. Hecht, and C. Pasold, "NLO QCD and electroweak corrections to W+γ production with leptonic W-boson decays", *JHEP* **04** (2015) 018, doi:10.1007/JHEP04(2015)018, arXiv:1412.7421.

[18] A. Denner, S. Dittmaier, M. Hecht, and C. Pasold, "NLO QCD and electroweak corrections to $Z + \gamma$ production with leptonic Z-boson decays", *JHEP* **02** (2016) 057, doi:10.1007/JHEP02(2016)057, arXiv:1510.08742.

[19] GEANT4 Collaboration, "GEANT4—a simulation toolkit", *Nucl. Instrum. Meth. A* **506** (2003) 250, doi:10.1016/S0168-9002(03)01368-8.

[20] J. Allison et al., "Geant4 developments and applications", *IEEE Trans. Nucl. Sci.* **53** (2006) 270, doi:10.1109/TNS.2006.869826.

[21] CMS Collaboration, "Measurement of the Inclusive W and Z Production Cross Sections in pp Collisions at $\sqrt{s} = 7$ TeV", *JHEP* **10** (2011) 132, doi:10.1007/JHEP10(2011)132, arXiv:1107.4789.

[22] A. Buckley et al., "LHAPDF6: parton density access in the LHC precision era", *Eur. Phys. J. C* **75** (2015) 132, doi:10.1140/epjc/s10052-015-3318-8, arXiv:1412.7420.

[23] CMS Collaboration, "CMS Luminosity Measurement for the 2015 Data Taking Period", CMS Physics Analysis Summary LUM-15-001, CERN, Geneva, 2016.